Biochemical and Biophysical Research Communications 451 (2014) 431–435

Contents lists available at ScienceDirect

Biochemical and Biophysical Research Communications

journal homepage: www.elsevier.com/locate/ybbrc

Structural insights into substrate specificity of crotonase from the *n*-butanol producing bacterium *Clostridium acetobutylicum*

Eun-Jung Kim [1], Yeo-Jin Kim [1], Kyung-Jin Kim *

School of Life Sciences, KNU Creative BioResearch Group, Kyungpook National University, Daehak-ro 80, Buk-ku, Daegu 702-701, Republic of Korea

ARTICLE INFO

Article history:
Received 24 July 2014
Available online 7 August 2014

Keywords:
Crotonase
3-Hydroxybutyryl-CoA dehydrogenase
n-Butanol
Clostridium acetobutylicum
Crystal structure

ABSTRACT

Crotonase from *Clostridium acetobutylicum* (*Ca*CRT) is an enzyme that catalyzes the dehydration of 3-hydroxybutyryl-CoA to crotonyl-CoA in the *n*-butanol biosynthetic pathway. To investigate the molecular mechanism underlying *n*-butanol biosynthesis, we determined the crystal structures of the *Ca*CRT protein in apo- and acetoacetyl-CoA bound forms. Similar to other canonical crotonase enzymes, *Ca*CRT forms a hexamer by the dimerization of two trimers. A crystal structure of *Ca*CRT in complex with acetoacetyl-CoA revealed that Ser69 and Ala24 to be signature residues of *Ca*CRT, which results in a distinct ADP binding mode wherein the ADP moiety is bound at a different position compared with other crotonases. We also revealed that the substrate specificity of crotonase enzymes is determined by both the structural feature of the α3 helix region and the residues contributing the enoyl-CoA binding pocket. A tight formed α3 helix and two phenylalanine residues, Phe143 and Phe233, aid *Ca*CRT to accommodate crotonyl-CoA as the substrate. The key residues involved in substrate binding, enzyme catalysis and substrate specificity were confirmed by site-directed mutagenesis.

1. Introduction

n-Butanol is a primary alcohol that, in compared to bio-ethanol, has high energy content, less corrosive nature, and less solubility in water, and is easier to blend with gasoline or diesel fuels. On the backdrop of worldwide issues such as global warming, energy security, and greenhouse effect, the desirable properties of *n*-butanol have led to growing research interest in the biological process underlying its production [1–3]. Once the key intermediate acetyl-CoA has been generated, it can be metabolized via three different pathways, producing acetone, ethanol, and butanol, in the so-called "acetone–butanol–ethanol (ABE)" fermentation [4,5]. It is been known that *n*-butanol is synthesized most actively from acetyl-CoA by the anaerobic bacteria of the genus *Clostridium* through six tightly regulated steps catalyzed by independent proteins [6]. For more than two decades, a large number of efforts ranging from genetic modifications to optimization of culture conditions have been made to improve *n*-butanol production in ABE fermentation. However, the final titer of *n*-butanol in heterologous host cells expressing whole clostridial *n*-butanol biosynthetic machinery has not exceeded 1 g/L [5,7–9].

Therefore, engineering of non-solventogens to produce a large amount of *n*-butanol remains a challenging task. First, among the several reasons that may be attributed to this challenge, the toxicity of *n*-butanol is toxic to bacterial cells [10]. For example, the growth of *Escherichia coli* cell is severely inhibited even in the presence of low concentrations of *n*-butanol and is almost completely repressed at *n*-butanol concentrations of approximately 1% (v/v) [8]. Second, additional pathways for *n*-butanol synthesis disrupt the balance of energy carriers such as NADH/NAD^+, which lowers the production of *n*-butanol [8]. In addition, anaerobic NADH generation is not sufficient for *n*-butanol production by *E. coli* [2,11]. Finally, since the activities of the heterologous enzymes involved in *n*-butanol synthesis are host-cell specific, each enzyme of the pathway needs to be optimized for expression in the heterologous host [9,10]. Therefore, detailed understanding of the function and regulation of key enzymes involved in the *n*-butanol biosynthetic pathway might be very important to rationally optimize heterologous metabolic pathways and maximize the *n*-butanol yield from engineered non-solventogenic microbes [12,13]. However, our understanding of the regulatory mechanisms of the enzymes involved in the *n*-butanol biosynthetic pathway in *Clostridium* is limited. With this background, further examination of the physiological characteristics of endogenous

* Corresponding author. Address: Structural and Molecular Biology Laboratory, School of Life Sciences, Kyungpook National University, Daehak-ro 80, Buk-ku, Daegu 702-701, Republic of Korea. Fax: +82 53 955 5522.
E-mail address: kkim@knu.ac.kr (K.-J. Kim).
[1] These authors contributed equally to this work.

http://dx.doi.org/10.1016/j.bbrc.2014.07.139
0006-291X/

n-butanol-producing organisms such as *Clostridium* spp. as well as non-solventogenic industrial microbes is necessary to increase *n*-butanol yield from naturally producing strains as well as from non-solventogenic industrial microbes.

Here we report the crystal structures of the apo- and substrate-bound form of crotonase from *Clostridium acetobutylicum* (*Ca*CRT), which converts 3-hydroxybutyryl-CoA to crotonyl-CoA by eliminating a proton and a hydroxyl group leading to the formation of a double bond at C2 and C3 of the enoyl moiety. Structural and biochemical studies reveal that *Ca*CRT possesses a peculiar substrate binding pocket that enables it to accommodate the four-carbon enoyl-CoA as its substrate.

2. Materials and methods

2.1. Preparation of CaCRT proteins

Cloning, expression, purification, and crystallization of *Ca*CRT will be described elsewhere (Kim et al., in preparation). Briefly, the *Ca*CRT coding gene (Met1-Arg261, M.W. 28 kDa) was amplified by polymerase chain reaction (PCR) using the chromosomal DNA of *C. acetobutylicum* strain ATCC 824 as a template. The PCR product was then subcloned into pET30a (Invitrogen) with 6*x*-histag at the C-terminus. The resulting expression vector pET30a:*CaCRT* was transformed into an *E. coli* B834 strain, which was grown in 1 L of LB medium containing kanamycin (50 μg/ml) at 37 °C. After induction via the addition of 1.0 mM IPTG, the culture medium was further maintained for 20 h at 18 °C. The culture was harvested by centrifugation at 5000×*g* at 4 °C. The cell pellet was resuspended in buffer A (40 mM Tris–HCl at pH 8.0 and 5 mM *β*-mercaptoethanol) and then disrupted by ultrasonication. The cell debris was removed by centrifugation at 11,000×*g* for 1 h, and lysate was bound to Ni–NTA agarose (QIAGEN). After washing with buffer A containing 20 mM imidazole, the bound proteins were eluted with 300 mM imidazole in buffer A. A trace amount of contamination was removed by applying HiLoad 26/60 Superdex 200 prep grade (GE Healthcare) size exclusion chromatography. The purified protein showed ~95% purity on SDS–PAGE, was concentrated to 20 mg/ml in 40 mM Tris–HCl, pH 8.0, 1 mM dithiothreitol (DTT). For the preparation of the *Ca*CRT mutant proteins, site-directed mutagenesis method was applied using the pET30a:*Ca*CRT plasmid as a template. The *Ca*CRT mutant proteins were prepared using the procedure same as the wild-type protein.

2.2. Crystallization and X-ray data collection

Suitable crystals for diffraction experiments were obtained at 22 °C within 5 days from the precipitant of 30% polyethyleneglycol 400, 0.1 M sodium cacodylate, pH 6.5, and 0.2 M lithium sulfate. The crystals were transferred to cryoprotectant solution containing 30% polyethyleneglycol 400, 0.1 M sodium cacodylate, pH 6.5, 0.2 M lithium sulfate, and 20% glycerol, fished out with a loop larger than the crystals and flash-frozen by immersion in liquid nitrogen at −173 °C. The data were collected to a resolution of 2.2 Å at 7A beamline of the Pohang Accelerator Laboratory (PAL, Pohang, Korea) using a Quantum 270 CCD detector (ADSC, USA). The data were then indexed, integrated, and scaled using the HKL2000 suite [14]. Crystals of an apo-form belonged to space group $P3_212$, with unit cell parameters of $a = b = 78.67$ Å and $c = 210.70$ Å. Assuming 3 molecules of *Ca*CRT per asymmetric unit, the crystal volume per unit of protein mass was 2.23 Å^3 kDa^{-1} [15], which corresponds to a solvent content of approximately 44.8%. *Ca*CRT crystals in complex with acetoacetyl-CoA were crystallized with the same crystallization condition supplemented with 20 mM acetoacetyl-CoA. Crystals in complex with acetoacetyl-CoA belonged to the space group $P3_212$ as well, with unit cell parameters similar to those of the apo-from of *Ca*CRT crystal.

Table 1
Data collection and refinement statistics.

	*Ca*CRT	
	Apo	Complex with CAA
Data collection		
Space group	$P3_212$	$P3_212$
Cell dimensions		
a, *b*, *c* (Å)	78.67, 78.67, 210.70	78.60, 78.60, 210.80
α, *β*, *γ* (°)	90.00, 90.00, 120.00	90.00, 90.00, 120.00
Resolution (Å)	50.00–2.20 (2.24–2.20) [a]	50.00–2.00 (2.03–2.00)
R_{sym} or R_{merge} [b]	6.8 (26.9)	8.7 (45.5)
$\langle I/\sigma(I)\rangle$	15.3 (2.3)	35.2 (4.1)
Completeness (%)	97.1 (89.3)	96.7 (98.0)
Redundancy	4.5 (2.8)	5.0 (3.9)
Refinement		
Resolution (Å)	50.00–2.20	50.00–2.00
No. reflections	35,417	46,614
R_{work}/R_{free} [c]	19.2/25.7	19.2/25.1
No. atoms	5866	6091
Protein	5727	5727
Ligand/ion	–	162
Water	139	202
Mean *B*-factors	35.2	41.9
Protein	35.1	39.7
CAA	–	140.5
Water	33.0	41.2
R.m.s. deviations		
Bond lengths (Å)	0.012	0.018
Bond angles (°)	1.569	1.976

[a] The numbers in parentheses are statistics from the highest resolution shell.
[b] $R_{sym} = \sum|I_{obs} - I_{avg}|/I_{obs}$, where I_{obs} is the observed intensity of individual reflection and I_{avg} is average over symmetry equivalents.
[c] $R_{work} = \sum||F_o| - |F_c||/\sum|F_o|$, where $|F_o|$ and $|F_c|$ are the observed and calculated structure factor amplitudes, respectively. R_{free} was calculated with 5% of the data.

2.3. Structure determination

The structure was determined by molecular replacement with the CCP4 version of MOLREP [16] using the *Rattus norvegicus* enoyl-CoA hydratase structure (PDB code 1MJ3) as a search model. The Model building was performed manually using the program WinCoot [17] and the refinement was performed with CCP4 refmac5 [18] and CNS [19]. The *Ca*CRT structure in complex with acetoacetyl-CoA was determined by molecular replacement with the CCP4 version of MOLREP using the apo-form of *Ca*CRT structure as a search model. Model building and structure refinement of the *Ca*CRT structure in complex with acetoacetyl-CoA were similarly performed with those of the apo-form of *Ca*CRT. The data statistics are summarized in Table 1.

2.4. Crotonase activity assay

For the crotonyl-CoA hydratase activity assay, the wild-type and mutant *Ca*CRT proteins (5 μM) were mixed the reaction buffer, containing 100 mM Tris–HCl pH 7.5 and crotonyl-CoA substrate (1–100 μM) (Sigma) at 25 °C. And hydration of crotonyl-CoA was measured by monitoring the decrease of absorbance at 263 nm. All experiments were performed in triplicate.

3. Results and discussion

3.1. Overall structure of CaCRT

To elucidate enzymatic properties of the *Ca*CRT protein, we determined its crystal structure at 2.2 Å. The crystal structure of *Ca*CRT in complex with acetoacetyl-CoA (AcAc-CoA) was also determined at 2.2 Å to define the substrate binding mode of the

enzyme (Fig. 1). The asymmetric unit of the crystal contained three *Ca*CRT molecules, corresponding to a trimer of the protein. The atomic structure was in good agreement with the X-ray crystallographic statistics of bond angles, bond lengths, and other geometric parameters (Table 1). The *Ca*CRT monomer consists of an N-terminal (NTD) and a C-terminal domains (CTD). The NTD (β1–β7 and α1–α9) harbors the canonical crotonase fold, where a large β-sheet (β1–β4 and β6) is organized with a small β-sheet (β5 and β7) forming two perpendicular β-sheets (Fig. 1B). The CTD consists of three α-helices (α10–α12), and this domain mediates the oligomerization of *Ca*CRT. Additionally, the extended α-helix (α12) interacts with the NTD of a neighboring monomer and participates in the formation of its substrate binding site (Fig. 1B).

Hexameric structure of *Ca*CRT could be easily generated by applying $P3_212$ crystallographic symmetric operation, which showed a dimer of two trimers (Fig. 1C). Size exclusion chromatography confirmed the hexameric nature of *Ca*CRT (data not shown). Trimer of *Ca*CRT is mediated by intimate contacts between 5 α-helices of the NTD of one polypeptide and the CTD of a neighboring polypeptide with approximately 2000 Å^2 surface area of each monomer buried at the trimer interface. The CTDs of six monomers participate mainly in the formation of the hexameric interface, which, in compared with the trimeric interface, is less extensive with approximately 1100 Å^2 surface area of each monomer buried at the interface.

3.2. Structural comparison to canonical crotonases

The overall structure of *Ca*CRT is similar to those of other crotonases. A search using the Dali server revealed that the structure of *Ca*CRT was homologous to that of rat liver enoyl-CoA hydratase (ECH) and *Ruegeria pomeroyi* methylthioacryloyl-CoA hydratase (DmdD) [20,21]. Despite similar structural fold and oligomeric status among these enzymes, the C-terminal loop (10 amino acids) is significantly different. The C-terminal loop of ECH is positioned distally from the bound CoA, while in DmdD it is located proximal to the bound CoA and is involved in the stabilization of the phosphate moiety of the substrate. However, because of a weak electron density map derived from both apo- and AcAc-bound structures of *Ca*CRT, the loop region could not be modeled, suggesting that this region in *Ca*CRT might not be involved in the stabilization of the phosphate moiety of the substrate (Fig. 2A).

3.3. The substrate binding pocket

The substrate binding mode of *Ca*CRT was elucidated based on the crystal structure of *Ca*CRT in complex with AcAc-CoA. The overall structure of the AcAc-CoA-bound form was almost identical to that of the apo-form of the enzyme. The substrate binding pocket is mainly constituted by residues of the small β-sheet and the loops near the sheet. The two terminal α-helices (α11 and α12) of a neighboring polypeptide also partially aid the formation of the substrate binding pocket (Fig. 2B). The pantothenic acid and acetoacetyl moieties are tightly bound and buried in the pocket, whereas the ADP moiety is partially exposed to the solvent. In the bound state, the bound AcAc-CoA is bent at an angle of 180° to the pyrophosphate moiety, resulting in a distance of approximately 5 Å between the adenine and the pantothenic acid moieties (Fig. 2B). Although the overall fold and the substrate binding site of *Ca*CRT are similar to those in ECH and DmdD, *Ca*CRT uses a unique CoA binding mode. The Ser69 residue in *Ca*CRT is hydrogen-bonded

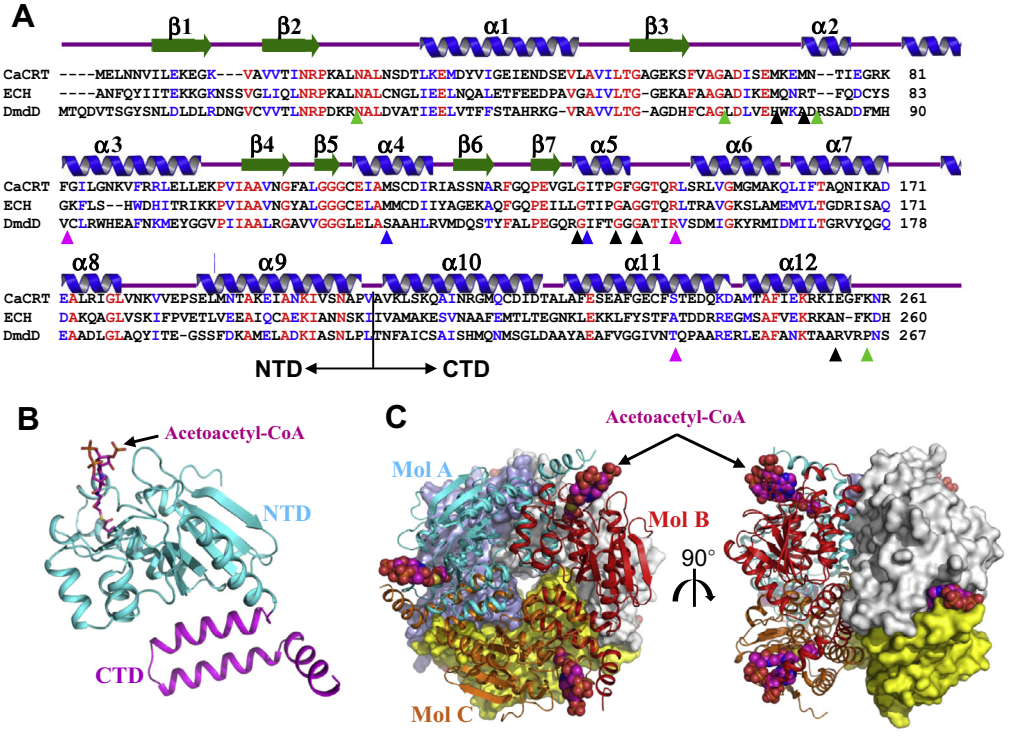

Fig. 1. Overall shape of *Ca*CRT. (A) Amino acid sequence alignment of crotonases. Secondary structure elements are shown based on the *Ca*CRT structure. Identical and highly conserved residues are presented in red and blue colored characters, respectively. Residues involved in the binding of ADP and pantothenic acid moieties are marked with green and black colored rectangles, respectively. Residues involved in the enzyme catalysis and the determination of the substrate specificity are marked with blue and magenta colored rectangles, respectively. Amino acid regions of NTD and CTD were indicated. (B) Monomeric structure of *Ca*CRT. Monomeric structure of *Ca*CRT was shown as a cartoon diagram, and the NTD and CTD were distinguished with cyan and magenta colors, respectively. The bound acetoacetyl-CoA was shown as a stick model with magenta color. (C) Hexameric structure of *Ca*CRT. One trimer was shown as a cartoon model, and another is as a surface model. Three molecules in one trimer was distinguished with different colors and labeled. Bound acetoacetyl-CoA was shown as a sphere model with magenta color. The right side figure is 180° rotated vertically from the left side figure. (For interpretation of the references to color in this figure legend, the reader is referred to the web version of this article.)

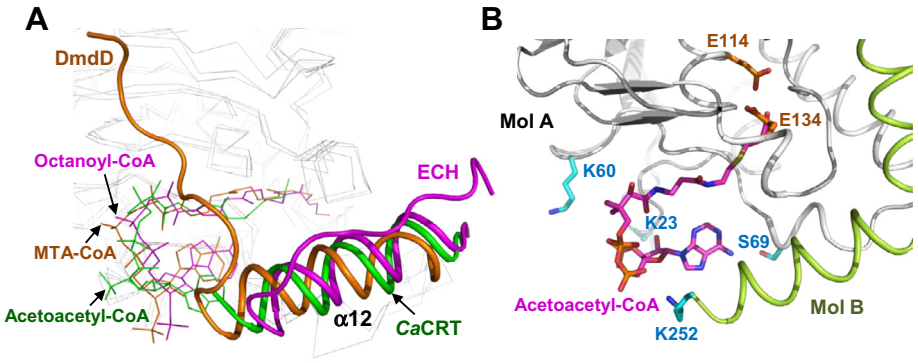

Fig. 2. Substrate binding site of *Ca*CRT. (A) Structural comparison of crotonases. Structures of three crotonases, *Ca*CRT, ECH, and DmdD, were superposed. Each polypeptide of three crotonases was presented with ribbon model with gray color, and the α3 helices of *Ca*CRT, ECH, and DmdD were shown as cartoon models with green, magenta, and orange colors, respectively, and labeled. The acetoacetyl-CoA, octanoyl-CoA, and MTA-CoA molecules bound to *Ca*CRT, ECH, and DmdD, were shown as stick models with green, magenta, and orange colors, respectively, and labeled. (B) Substrate binding mode of *Ca*CRT. The *Ca*CRT structure was shown as a cartoon model. One polypeptide was shown with gray color, and the neighboring polypeptide was with lime color. The bound acetoacetyl-CoA was shown as a stick model with magenta color. Two catalytic residues, E114 and E134, were shown as a stick model with orange color, and the residues involved in the ADP binding were with cyan color. (For interpretation of the references to color in this figure legend, the reader is referred to the web version of this article.)

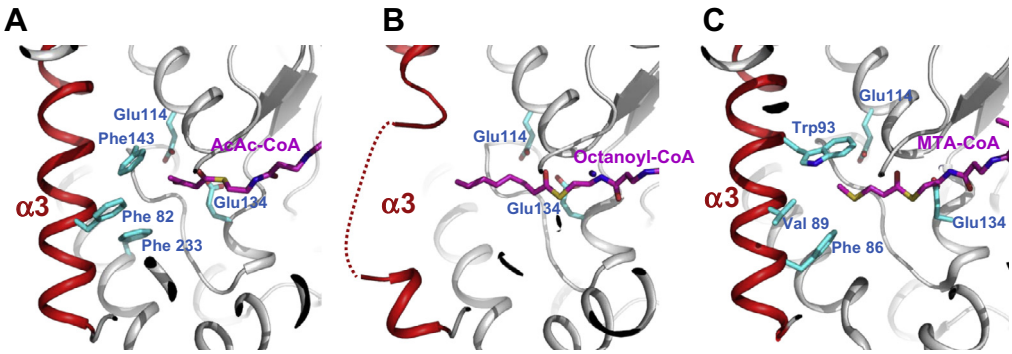

Fig. 3. Substrate specificity of crotonases. Regions determining substrate specificity in CaCRT (A), ECH (B), and DmdD (C) were presented with cartoons models with gray color. The α3 helix of the three enzymes were highlighted with red color and labeled. The residues involved in the enzyme catalysis and the constitution of the enoyl moiety binding pocket were shown as stick models with cyan color, and labeled appropriately. The bound substrate or inhibitors, AcAc-CoA, octanoyl-CoA, and MTA-CoA, of *Ca*CRT, ECH, and DmdD, respectively, were shown as stick models with magenta color. The flexible region in the α3 helix of ECH was indicated with dotted line. (For interpretation of the references to color in this figure legend, the reader is referred to the web version of this article.)

with N6 of AcAc-CoA, in contrast to the corresponding Lys101 and Val74 residues in ECH and DmdD, and is involved in the stabilization of the adenine ring. Moreover, Ala24 of *Ca*CRT is located near the phosphate moiety, whereas the corresponding Lys31 residue of DmdD is hydrogen-bonded with this moiety. These differences resulted in the ADP moiety being bound in a distinct position, which is more distal from the pantothenic acid moiety compared to that in ECH and DmdD (Fig. 2A). Three lysine residues, namely Lys23, Lys60, and Lys252, are also positioned near the ADP moiety and seem to be involved in the stabilization of the pyrophosphate moiety in *Ca*CRT (Fig. 2B). In order to investigate the contribution of specific residues involved in ADP binding in *Ca*CRT, we performed structure-based site-directed mutagenesis and generated four mutants (K23A, K60A, S69A, and K252A). Compared to the wild-type, the K23A and S69A mutants showed complete loss of enzyme activity, indicating that Lys23 and Ser69 are the key residues involved in stabilizing the ADP moiety. On the other hand, the K60A mutant showed 50% enzymatic activity, indicating the partial involvement of the Lys60 residue in the stabilization of the pyrophosphate moiety. More interestingly, the K252A mutant exhibited a 1.5-fold higher activity compared to the wild-type protein. We speculate that an increase in the hydrophobicity of the Lys252 surface region upon replacement with alanine might result in a more favorable environment for the binding of the adenosine moiety (Fig. 4). The pantothenic acid moiety is stabilized via hydrogen bonding to the main chain of Gly65 and van der Waals interactions with several hydrophobic residues such as Ile68, Pro133, Leu137, Ile139, and Phe249. We suspected that the two conserved glutamate residues, Glu114 and Glu134, present at the active site of *Ca*CRT and located near the C1 and C2 of fatty acid moiety might be utilized for the enzyme catalysis functioning as the general base and general acid, respectively, as proposed for other canonical crotonase enzymes (Fig. 2B) [22,23]. A complete loss of enzyme activity in the E114A and E134A mutants confirmed their involvement in enzyme catalysis (Fig. 4).

3.4. Structural features for substrate specificity

Although crotonase enzymes catalyze a hydration reaction by using various types of enoyl-CoAs as substrates, their substrate specificities are quite different from each other. For example, it is known that three crotonase enzymes, *Ca*CRT, ECH and DmdD, use crotonyl-CoA, enoyl-CoAs with various lengths of the carbon chain, and methylthioacryloyl-CoA (MTA-CoA) as a substrate, respectively. These substrate specificities can be explained by structural comparison of the enoyl moiety binding pockets of these enzymes. Compared to ECH where the α3 helix is highly flexible, especially in the region from Ser113 to His119 residues, the corresponding

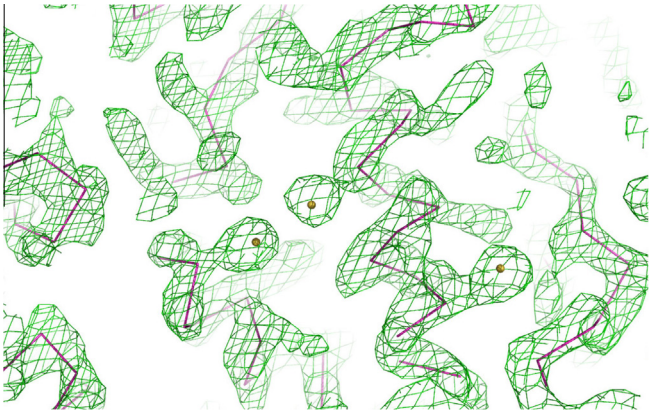

Fig. 4. Site-directed mutagenesis experiments of *Ca*CRT. Residues involved in enzyme catalysis, substrate specificity, and substrate binding were replaced by alanine residues. The relative activities of recombinant mutant proteins were measured and compared with that of the wild-type *Ca*CRT.

helix in *Ca*CRT is tightly formed (Fig. 3A and B). We suspect that such a tightly-formed α3 helix in *Ca*CRT enables it to constitute a well-organized pocket to perfectly fit the four-carbon crotonyl-CoA, whereas the flexible structure at the α3 helix in ECH provides a spatial flexibility for accommodating enoyl-CoAs with various lengths of carbon chain. In fact, the crotonyl moiety binding pocket in *Ca*CRT is constituted by three phenylalanine residues, Phe82, Phe143 and Phe233, of which the Phe82 residue is located at the α3 helix (Fig. 3A). In DmdD, the α3 helix is also tightly formed, however, the binding pocket for methylthioacryloyl moiety is organized by completely different residues such as Phe86, Val89, Trp93, and Gly150 which aid in accommodating methylthioacryloyl moiety that is somewhat larger than the crotonyl moiety (Fig. 3C). We performed site-directed mutagenesis to test if the three unique phenylalanine residues (Phe82, Phe143 and Phe233) were involved in the constitution of the crotonyl binding pocket in *Ca*CRT. Interestingly, the F82A mutant showed similar enzyme activity compared with the wild-type, whereas the F143A and F233A mutants exhibited almost complete loss of activity (Fig. 4). These results indicate that Phe143 and Phe233 are key residues for the constitution of the crotonyl binding pocket to accommodate the four-carbon crotonyl-CoA as a substrate.

Acknowledgments

This work was supported by the National Research Foundation of Korea (NRF) Grant funded by the Korean Government (MEST) (NRF-2009-C1AAA001-2009-0093483, and NRF-2014M1A2A2 033626) and by the Advanced Biomass R&D Center (ABC) of Global Frontier Project funded by the MEST (ABC-2012-053895).

References

[1] P. Durre, Fermentative butanol production: bulk chemical and biofuel, Ann. N. Y. Acad. Sci. 1125 (2008) 353–362.
[2] P. Durre, Biobutanol: an attractive biofuel, Biotechnol. J. 2 (2007) 1525–1534.
[3] S.Y. Lee, J.H. Park, S.H. Jang, L.K. Nielsen, J. Kim, K.S. Jung, Fermentative butanol production by clostridia, Biotechnol. Bioeng. 101 (2008) 209–228.
[4] W.J. Mitchell, Physiology of carbohydrate to solvent conversion by clostridia, Adv. Microb. Physiol. 39 (1998) 31–130.
[5] M. Inui, M. Suda, S. Kimura, K. Yasuda, H. Suzuki, H. Toda, S. Yamamoto, S. Okino, N. Suzuki, H. Yukawa, Expression of *Clostridium acetobutylicum* butanol synthetic genes in *Escherichia coli*, Appl. Microbiol. Biotechnol. 77 (2008) 1305–1316.
[6] D.T. Jones, D.R. Woods, Acetone-butanol fermentation revisited, Microbiol. Rev. 50 (1986) 484–524.
[7] D.R. Nielsen, E. Leonard, S.H. Yoon, H.C. Tseng, C. Yuan, K.L. Prather, Engineering alternative butanol production platforms in heterologous bacteria, Metab. Eng. 11 (2009) 262–273.
[8] S. Atsumi, T. Hanai, J.C. Liao, Non-fermentative pathways for synthesis of branched-chain higher alcohols as biofuels, Nature 451 (2008) 86–89.
[9] E.J. Steen, R. Chan, N. Prasad, S. Myers, C.J. Petzold, A. Redding, M. Ouellet, J.D. Keasling, Metabolic engineering of *Saccharomyces cerevisiae* for the production of n-butanol, Microb. Cell Fact. 7 (2008) 36.
[10] S.A. Nicolaou, S.M. Gaida, E.T. Papoutsakis, A comparative view of metabolite and substrate stress and tolerance in microbial bioprocessing: From biofuels and chemicals, to biocatalysis and bioremediation, Metab. Eng. 12 (2010) 307–331.
[11] S. Atsumi, A.F. Cann, M.R. Connor, C.R. Shen, K.M. Smith, M.P. Brynildsen, K.J. Chou, T. Hanai, J.C. Liao, Metabolic engineering of *Escherichia coli* for 1-butanol production, Metab. Eng. 10 (2008) 305–311.
[12] S.K. Lee, H. Chou, T.S. Ham, T.S. Lee, J.D. Keasling, Metabolic engineering of microorganisms for biofuels production: from bugs to synthetic biology to fuels, Curr. Opin. Biotechnol. 19 (2008) 556–563.
[13] E.A. Felnagle, A. Chaubey, E.L. Noey, K.N. Houk, J.C. Liao, Engineering synthetic recursive pathways to generate non-natural small molecules, Nat. Chem. Biol. 8 (2012) 518–526.
[14] Z. Otwinowski, W. Minor, Processing of X-ray diffraction data collected in oscillation mode, Macromol. Crystallogr., Pt A 276 (1997) 307–326.
[15] B.W. Matthews, Solvent content of protein crystals, J. Mol. Biol. 33 (1968) 491–497.
[16] A. Vagin, A. Teplyakov, Molecular replacement with MOLREP, Acta Crystallogr. D Biol. Crystallogr. 66 (2010) 22–25.
[17] K. Cowtan, P. Emsley, Coot: model-building tools for molecular graphics, Acta Crystallogr. D Biol. Crystallogr. 60 (2004) 2126–2132.
[18] G.N. Murshudov, A.A. Vagin, E.J. Dodson, Refinement of macromolecular structures by the maximum-likelihood method, Acta Crystallogr. D Biol. Crystallogr. 53 (1997) 240–255.
[19] A.T. Brunger, P.D. Adams, G.M. Clore, W.L. DeLano, P. Gros, R.W. Grosse-Kunstleve, J.S. Jiang, J. Kuszewski, M. Nilges, N.S. Pannu, R.J. Read, L.M. Rice, T. Simonson, G.L. Warren, Crystallography & NMR system: a new software suite for macromolecular structure determination, Acta Crystallogr. D Biol. Crystallogr. 54 (1998) 905–921.
[20] C.R. Reisch, M.J. Stoudemayer, V.A. Varaljay, I.J. Amster, M.A. Moran, W.B. Whitman, Novel pathway for assimilation of dimethylsulphoniopropionate widespread in marine bacteria, Nature 473 (2011) 208–211.
[21] D. Tan, W.M. Crabb, W.B. Whitman, L. Tong, Crystal structure of DmdD, a crotonase superfamily enzyme that catalyzes the hydration and hydrolysis of methylthioacryloyl-CoA, PLoS One 8 (2013) e63870.
[22] B.J. Bahnson, V.E. Anderson, G.A. Petsko, Structural mechanism of enoyl-CoA hydratase: three atoms from a single water are added in either an E1cb stepwise or concerted fashion, Biochemistry 41 (2002) 2621–2629.
[23] H.A. Hofstein, Y. Feng, V.E. Anderson, P.J. Tonge, Role of glutamate 144 and glutamate 164 in the catalytic mechanism of enoyl-CoA hydratase, Biochemistry 38 (1999) 9508–9516.